







[View Journal Online](#)  
[View Article Online](#)

# Comprehensive DFT analysis of BeHfO<sub>3</sub> perovskite: Exploring the structure, mechanical, thermodynamic, and optic properties

Md Al Masud <sup>1</sup>, Md. Rajib Munshi <sup>2,\*</sup>, Tanvir Chowdhury <sup>3</sup>,  
Mita Chakraborty <sup>2</sup> and Rakibul Islam <sup>4</sup>

<sup>1</sup> Department of Industrial and Production Engineering, Faculty of Science and Engineering, European University of Bangladesh, Dhaka-1216, Bangladesh

<sup>2</sup> Department of Physics, Faculty of Science and Engineering, European University of Bangladesh, Dhaka-1216, Bangladesh

<sup>3</sup> Department of Applied Physics and Electronics, Faculty of Science and Engineering, Jahangirnagar University, Savar, Dhaka -1342, Bangladesh

<sup>4</sup> Department of Controller of Examinations, European University of Bangladesh, Dhaka-1216, Bangladesh

\* Corresponding author at: Department of Physics, Faculty of Science and Engineering, European University of Bangladesh, Dhaka-1216, Bangladesh.  
e-mail: [razibmunshi@eub.edu.bd](mailto:razibmunshi@eub.edu.bd) (M.R. Munshi).

## RESEARCH ARTICLE



doi: 10.5155/eurjchem.16.3.292-301.2675

Received: 24 February 2025

Received in revised form: 1 June 2025

Accepted: 29 June 2025

Published online: 30 September 2025

Printed: 30 September 2025

## KEYWORDS

Elastic  
Optical  
Structural  
Electronic  
Absorption  
Photocatalyst

## ABSTRACT

We performed a thorough study of the electronic, mechanical, thermodynamic, and optical properties of the BeHfO<sub>3</sub> perovskite crystal using first-principles calculations featuring density functional theory (DFT). Electronic band structure analysis manifested the material to be semiconducting in nature with calculated band gap values of 0.873 eV (PBE), 0.887 eV (RPBE), 0.781 eV (PBEsol), 0.890 eV (LDA), 1.71 eV (HSE06) and 2.925 eV (B3LYP), reflecting considerable uncertainty in terms of exchange-correlation functionals and emphasizing the utility of hybrid functionals in estimating the band gap. Density of states (DOS) and partial density of states (PDOS) analyses were vital in revealing the role of the participating atoms (Be, Hf, and O) in electronic contribution, orbital hybridization, and the major states close to the Fermi level, highlighting the dominant states near the Fermi level and the role played by them in bonding. The Mulliken population analysis also described the electrostatic interaction and charge reorganization, confirming the mixed ionic-covalent nature of the bonds and revealing the complexity in the nature of bonds in the BeHfO<sub>3</sub> lattice. Mechanical stability was thoroughly analyzed using the Born mechanical stability criteria (BMS) which validated the mechanical stability of the compound. The calculation of the elastic constants helped to establish Poisson's ratio and Pugh's modulus ratio (B/G) to confirm the mechanical strength and ductility of the compound along with the pronounced anisotropy in the elastic properties, which could be valuable in applications requiring directional devices. The calculation of the optical properties in terms of the frequency-dependent dielectric functions and the absorption coefficients using different DFT approaches proved the material to be a powerful absorber in both the ultraviolet (UV) and visible parts of the spectrum, which establishes the material as a valuable contender in the field of optoelectronic and photocatalytic technology.

Cite this: *Eur. J. Chem.* 2025, 16(3), 292-301

Journal website: [www.eurjchem.com](http://www.eurjchem.com)

## 1. Introduction

The investigation and identification of semiconductor materials with innovative and unexplored characteristics have been propelled by the growing necessity to commercialize breakthrough technology. Numerous materials that had been neglected until recently after discovery are now receiving renewed attention due to their potential practical uses [1,2]. Oxide-based compounds have a broad range of characteristics and are promising for several technical applications, including refractory ceramics, superconductors, ferroelectrics, and solar energy materials. Their applications include solid oxide fuel cells, sensors, random access memory, high-density capacitors, catalysts, magnets, and high k dielectrics [3-5]. BeHfO<sub>3</sub> has been proven to be effective as a ceramic substrate of high k dielectric capacitor, thermal insulator and scintillator in rapid response detectors, attributed to its solid phase stability, elevated melting point, high thermal expansion coefficient, low thermal

conductivity and substantial density [6-9]. The static dielectric constant, a crucial metric for device manufacturing, is often elevated in these materials, thus improving their functional performance. Transition-metal oxides are distinguished by their photocatalytic activity, photoluminescence, and increased chemical reactivity, increasing their utility [10]. Perovskite materials, characterized by the general formula ABX<sub>3</sub>, have attracted considerable interest for their many applications in semiconductors, energy storage, and optoelectronics [11]. Halide perovskites are particularly attractive because of their adjustable bandgaps and elevated absorption coefficients, making them suitable for use in solar cells, light-emitting diodes (LEDs), and scintillators. However, concerns about lead toxicity and environmental instability have restricted their commercial use. This has inspired theoretical investigations into lead-free halide perovskites, including LiBeCl<sub>3</sub> and LiMgCl<sub>3</sub> [12,13].

**Table 1.** Optimized lattice parameter, cell volume, and final energy of BeHfO<sub>3</sub> crystal.

Compound	Lattice parameter $a=b=c$ (Å)	Initial cell volume (Å <sup>3</sup> )	Optimized cell volume (Å <sup>3</sup> )	Final energy (eV)	Methods
BeHfO <sub>3</sub>	3.346402	54.010152	37.474382	-1410.976738180	PBE
	3.356706	54.010152	37.821604	-1411.855961562	RPBE
	3.334390	54.010152	37.072281	-1407.297375017	PBE sol
	3.317263	54.010152	36.503941	-1410.935450263	LDA
	3.780	54.010152	54.112	-1405.541434666	B3LYP

Density Functional Theory (DFT) analyses demonstrate that these materials possess broad indirect bandgaps, dynamic stability, and advantageous optical characteristics, suggesting their potential for optoelectronic applications such as energy storage and scintillation devices. Oxide perovskites have garnered scientific attention due to their structural stability and broad bandgaps, making them suitable for use in lenses, lithography, and energy storage. Silicon-based oxide perovskites, including SiMO<sub>3</sub> (M: Sn, Ge), demonstrate mechanical stability and semiconductor properties, with band gaps appropriate for ultraviolet (UV) applications [14,15]. Recent computational investigations employing DFT have focused on silicon-based XSiO<sub>3</sub> (X: Sc, Y) compounds, emphasizing their advantageous structural, elastic, electrical, and optical properties for optoelectronic applications [16]. Computational studies of CaQCl<sub>3</sub> (Q: Li, K) chloroperovskites have disclosed favorable structural, elastic, electrical, and optical features for these applications [17]. Ti-based fluoro-perovskites (*e.g.*, TiVF<sub>3</sub> and TiNbF<sub>3</sub>) have semiconducting properties, mechanical stability, and ferromagnetism, rendering them viable candidates for optoelectronic and photovoltaic applications [18]. The structural adaptability and compositional variety of perovskite materials provide an extensive array of mechanical, electrical, magnetic, optical, and transport capabilities, permitting their application in domains such as optoelectronics, photonics, and spintronics. Chloroperovskites, containing chlorine as the halogen, exhibit broad band gaps, ideal for ultraviolet light applications and energy storage. They also possess ferroelectric and semiconductive properties beneficial for scintillating materials in medical imaging and high-energy physics [19,20].

Although comprehensive theoretical investigations have been performed on different aspects of several semiconductors, including BaHfO<sub>3</sub> [21,22], CaHfO<sub>3</sub>, and SrHfO<sub>3</sub> [23,24], the compound BeHfO<sub>3</sub> has not been thoroughly examined. Due to the prevalent application of Hf-based high-k dielectrics such as HfO<sub>2</sub> in contemporary electronics, BeHfO<sub>3</sub> emerges as a viable alternative with distinctive characteristics. The photocatalytic uses of hafnia derivatives have recently attracted attention; however, the potential of BeHfO<sub>3</sub> in this domain remains inadequately explored. The capacity to adjust the optical bandgap in these materials presents significant possibilities for enhancing photocatalysts. Hybrid Density Functional Theory (Hybrid-DFT) techniques offer the most precise framework for forecasting the electrical and structural characteristics of semiconductors, addressing the shortcomings of traditional DFT methodologies [25]. As far as current understanding goes, there are no theoretical investigations into its physical properties. However, one of the most effective methods to perform theoretical assessments of these features is first-principles computation. Rapid computational execution and somewhat precise predictions of the structural and energetic characteristics of various materials are the primary grounds for the utilization of LDA and GGA functionals [26].

In this study, the physical characteristics of BeHfO<sub>3</sub> perovskite were investigated employing a variety of exchange correlation functionals within the context of density functional theory (DFT) under the CASTEP module in Materials Studio. Some of the functionals that were chosen include the Generalized Gradient Approximation (GGA) with Perdew-Burke-Ernzerhof (PBE), the Local Density Approximation

(LDA) with Ceperley-Alder and Perdew-Zunger (CA-PZ), and the hybrid HSE06, B3LYP functional. The structural, electrical, mechanical, thermodynamic, and optical characteristics of the compound may be thoroughly examined using this multi-functional method, which allows for an evaluation of the changes based on the functions. Each function affects the precision of the findings in a distinct way. GGA-PBE and its variations (RPBE and PBESol) are widely utilized to predict structural and elastic characteristics; nevertheless, they often underestimate band gaps and marginally overestimate lattice parameters. LDA (CA-PZ) often yields more compact structures, owing to its underestimating of lattice constants. On the contrary, the HSE06 and B3LYP hybrid functional, which includes a fraction of exact exchange, yields more precise electronic structure predictions, especially for band gap values, while it incurs a greater computational expense. The use of several functionals enhances the dependability of results and elucidates the sensitivity of anticipated features to the selection of an exchange-correlation functional, hence facilitating a more robust interpretation of material behavior.

## 2. Computational method

The ab initio calculations in this study were performed using the CASTEP code within the Materials Studio package. A plane-wave basis set with a cutoff energy of 450 eV was used along with norm-conserving pseudopotentials. A  $6 \times 6 \times 6$  Monkhorst-Pack k-point grid was employed to ensure accurate Brillouin zone sampling. The geometry optimization convergence criteria were found to be total energy tolerance:  $2.0 \times 10^{-4}$  eV/atom, maximum ionic force:  $5.0 \times 10^{-2}$  eV/Å, maximum stress:  $1.0 \times 10^{-1}$  GPa, maximum atomic displacement:  $2.0 \times 10^{-3}$  Å.

## 3. Results and discussion

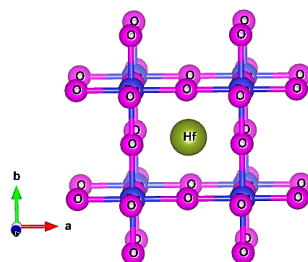
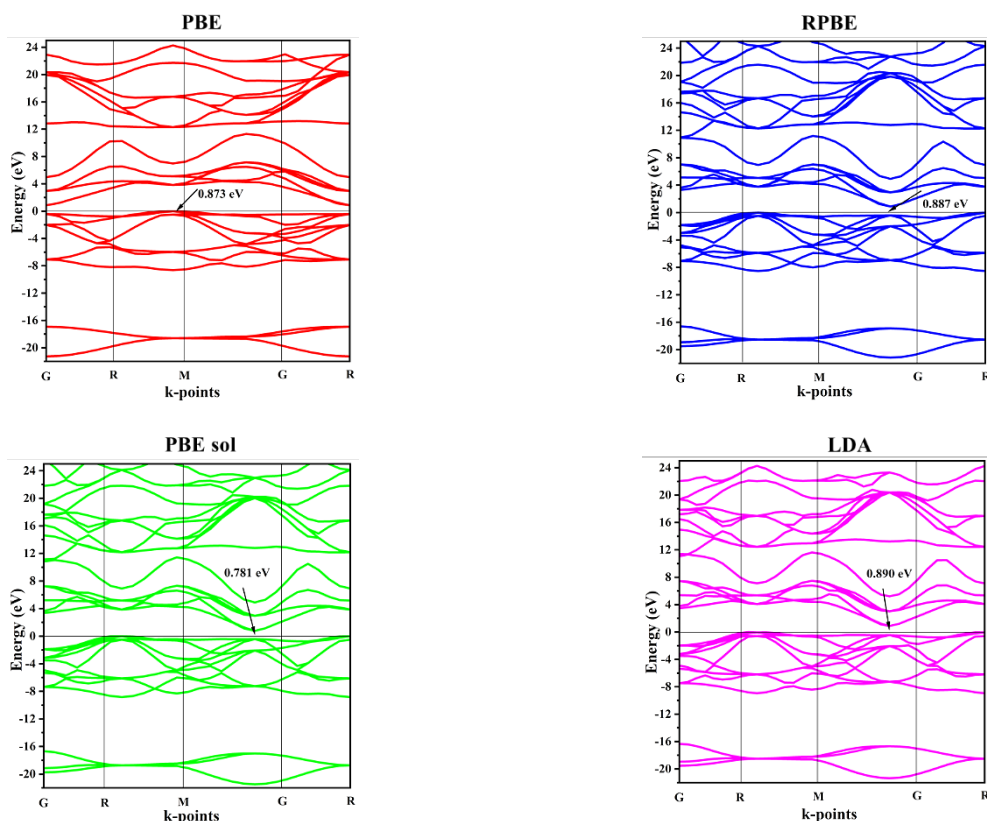
### 3.1. Optimization of crystal structure

We performed full structural optimization of the BeHfO<sub>3</sub> crystal prior to DFT calculations. The initial lattice parameters ( $a = b = c = 3.780$  Å;  $\alpha = \beta = \gamma = 90^\circ$ ) were taken from previous literature [20], and the structure was optimized to its ground state using DFT. The final configuration retained the cubic symmetry (space group *Pm3m* [221]), confirming the stability of the structure. This procedure ensures the reliability of the calculated properties.

The Hall symbol -P423 represents the crystal system, providing further information about it. The conclusive configuration of the BeHfO<sub>3</sub> crystals is showed in Table 1 and illustrated in Figure 1. The data presented in Table 1 were obtained through full structural optimization of the BeHfO<sub>3</sub> crystal using density functional theory (DFT) with different exchange-correlation functionals (PBE, RPBE, PBESol, LDA, and B3LYP). The initial lattice parameters ( $a = b = c = 3.780$  Å) were taken from the literature [20], and each structure was relaxed to its ground state by minimizing the total energy and atomic forces. For each functional, we report the optimized lattice parameter ( $a = b = c$ ), the corresponding cell volume after relaxation, and the final total energy.

**Table 2.** Band gap values of the BeHfO<sub>3</sub> crystal.

Band gap energy (eV)					
PBE	RPBE	PBE sol	LDA	HSE06	B3LYP
0.873	0.887	0.781	0.890	1.71	2.925

**Figure 1.** Structure (ball and stick) of cubic BeHfO<sub>3</sub> crystal.**Figure 2.** Band structure of BeHfO<sub>3</sub> using (a) PBE, (b) RPBE, (c) PBEsol and (d) LDA techniques.

The initial cell volume (54.010 Å<sup>3</sup>) was calculated based on the non-optimized lattice parameter, and the changes after optimization reflect the degree of structural relaxation. These calculations confirm the most stable structure and ensure the reliability of further property predictions.

### 3.2. Electronic band structure

Significant for assessing electrical characteristics, the layout of bands reveals significant details on the energetic concentrations and band widths of an object. Band structures of cubic BeHfO<sub>3</sub> at various high-symmetry points within the Brillouin zone, particularly at the (G-R-M-G-R) spot. Computing methods such as PBE, RPBE, PBEsol, LDA are presented in Figure 2, B3LYP (Figure S1, ESI) and HSE06 (Figure S2, ESI) were used to determine the minuscule band gap widths that characterize the spectrum of BeHfO<sub>3</sub>, indicating that it behaves like a semiconductor. The difference between a direct and

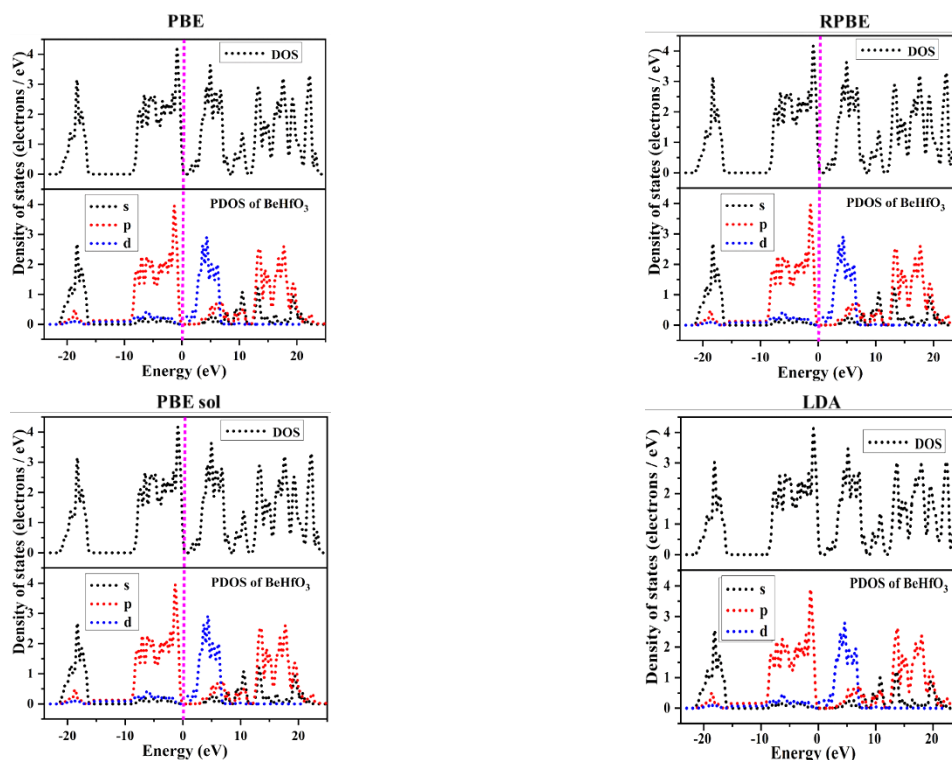
indirect band gap is the degree to which the energies of the conduction and valence bands coincide at the identical k-point [27-29]. The findings of our computational analysis demonstrate that BeHfO<sub>3</sub> has an indirect band gap, as illustrated in Table 2.

The valence band will display a significant number of occupied electronic states, while the conduction band will show a lower number of accessible unoccupied states in the density of states [30]. The plot of electronic states for a metal will exhibit a uniform distribution across a broad spectrum of energies. From Figure 3, and (Figure S3, ESI) it has been seen that, valence and conduction band level the highest DOS peak level reached near about 4.00 and 3.8 electrons/eV.

On the other hand, in Figure 4 and (Figure S4, ESI) for PDOS, valence band of Be and Hf atom partially dominated by 2s<sup>2</sup>, 5p<sup>2</sup> and 5d<sup>2</sup> orbital, respectively, while conduction band, the 2s<sup>2</sup> orbital of the Be atom, along with the 5p<sup>2</sup> and 5d<sup>2</sup> orbitals of the Hf atom, and the 2p<sup>2</sup> orbital of the O atom, exhibit the most

**Table 3.** Mulliken atomic population analysis of BeHfO<sub>3</sub> perovskites.

Methods	Mulliken Element	Charge	Bonds	Populations	Bond length (Å)	Hirshfeld Charge
PBE	Be	0.37	Be - O	0.75	1.67320	0.07
	Hf	1.92	Hf - O	0.60	2.36626	0.68
	O	-0.76	O - O	-0.46	2.36626	-0.25
			Be - Hf	-0.84	2.89807	-
RPBE	Be	0.38	Be - O	0.74	1.67835	0.07
	Hf	-0.77	Hf - O	0.61	2.37355	-0.25
	O	1.91	O - O	-0.46	2.37355	0.69
			Be - Hf	-0.77	2.90699	-
PBE sol	Be	0.32	Be - O	0.77	1.66720	0.06
	Hf	1.90	Hf - O	0.60	2.35777	0.65
	O	-0.74	O - O	-0.48	2.35777	-0.24
			Be - Hf	-0.93	2.88767	-
LDA	Be	0.30	Be - O	0.78	1.65863	0.07
	Hf	1.99	Hf - O	0.57	2.34566	0.67
	O	-0.76	O - O	-0.49	2.34566	-0.25
			Be - Hf	-1.03	2.87283	-

**Figure 3.** Total DOS and PDOS of BeHfO<sub>3</sub> using the (a) PBE (b) RPBE, (c) PBE sol, and (d) LDA techniques.

significant contributions. Lastly, about 3.8 electrons/eV are significantly contributed by the p orbital in the valence band. With almost four electrons/eV, the d orbital makes a substantial contribution to the conduction spectrum [31].

A study of the Mulliken atomic population is also included to supplement the investigation of the bridging features of the BeHfO<sub>3</sub> crystal. The veracity of our knowledge of charge transporters and the interactions between atoms in different compounds is verified by studies [32]. The atomic charges of oxygen (O) are negative, whereas those of beryllium (Be) and hafnium (Hf) are positive. Table 3, details the attributes of the BeHfO<sub>3</sub> crystal as evaluated using the PBE, RPBE, PBEsol, and LDA techniques. Additionally, the oxygen atom received a charge from the beryllium and hafnium atoms, resulting in an electric charge swap.

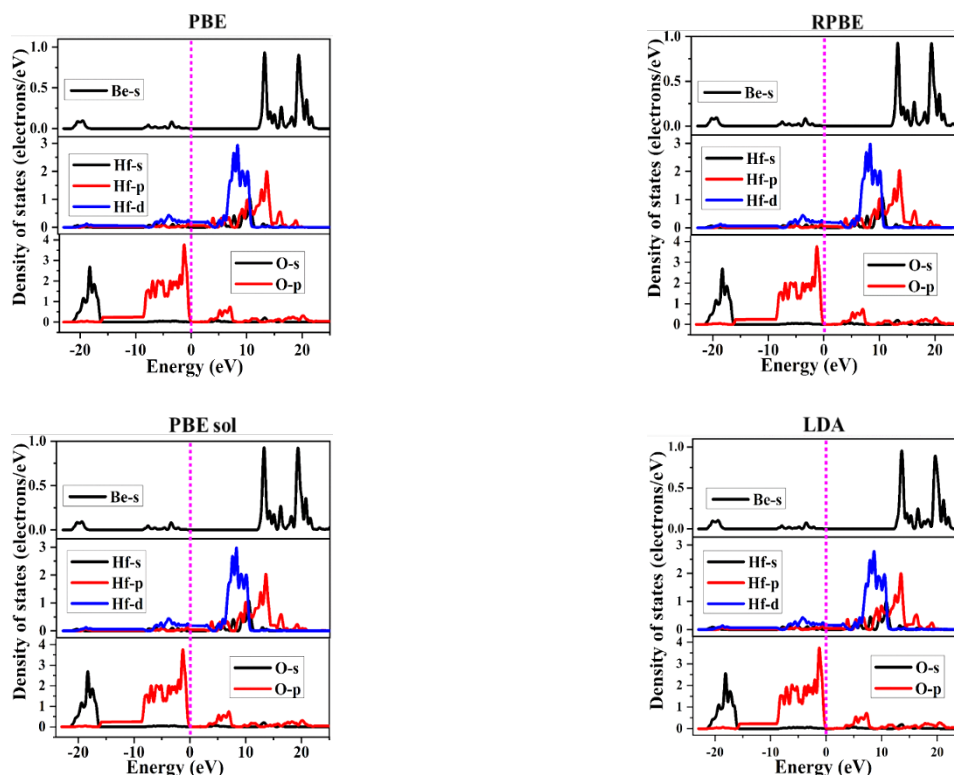
### 3.3. Mechanical properties

The elastic constant quantifies a material's susceptibility to deformation, indicating its reaction to tension, compression,

and distortion. Elastic constants were calculated utilizing Hooke's law and stress-strain data. For cubic crystals, mechanical stability requires adherence to the Born stability criteria [33]:  $C_{11} > 0$ ,  $C_{44} > 0$ ,  $C_{11} - C_{12} > 0$ , and  $C_{11} + 2C_{12} > 0$ . Table 5, presents the mechanical characteristics of BeHfO<sub>3</sub> as determined by PBE, RPBE, and PBEsol, therefore affirming its stability under these circumstances. Mechanical parameters such as elastic constants, bulk modulus, shear modulus, Young's modulus, and Poisson's ratio characterize the material's response to applied stress or strain. These parameters are intrinsically linked to the nature of atomic bonding within the material. The atoms in materials with strong covalent bonding are so closely linked that they resist deformation, making the material very stiff and having a large elastic modulus. The directed structures of the ionic bonding and electrostatic interactions cause them to be somewhat stiff, but they are frequently fragile. Because of the delocalized electron cloud that allows for atomic mobility, metallic bonds are linked to excellent ductility and moderate to high elastic moduli. Low elastic moduli and greater deformability are characteristics of

**Table 4.** Comparison with related materials predicted by the DFT study.

Compound	Cutt off energy & K-points	Crystal system with space group	Lattice parameter (Å)	Band gap (eV)	Software package	Reference
BaHfO <sub>3</sub>	E <sub>Cut</sub> = 450 eV K = 6 6 6	Cubic (pm3m)	4.2481	2.99 (LDA)	Material Studio-Castep	[21]
BaHfO <sub>3</sub>	E <sub>Cut</sub> = 380 eV K = 6 6 6	-	a = b = c = 4.24	2.99 (LDA)	Material Studio-Castep	[22]
CaHfO <sub>3</sub>	-	Cubic (pm3m)	4.16	3.77 (SCAN) 5.81 (TB-mBJ)	WIEN2k	[23]
SrHfO <sub>3</sub>	-	Cubic (pm3m)	4.11	4.01 (SCAN) 6.34 (TB-mBJ)	WIEN2k	[23]
SrHfO <sub>3</sub>	K = 4 4 3	Orthorombic (pbnm)	a = 5.86, b = 5.89, c = 8.28	3.4 (LDA)	Material Studio-Castep	[24]
BeHfO <sub>3</sub>	E <sub>Cut</sub> = 450 eV K = 6 6 6	Cubic (pm3m)	a = b = c = 3.780 $\alpha = \beta = \gamma = 90^\circ$	0.873 (PBE) 0.887 (RPBE) 0.781 (PBE sol) 0.890 (LDA) 2.925 (B3LYP) (HSE06)	Material Studio-Castep	This work

**Figure 4.** Different partial states of Be, Hf and O atom using the (a) PBE (b) RPBE (c) PBE sol (d) LDA techniques.

materials in which van der Waals or other weak interactions predominate. As a result, evaluation of mechanical parameters is a powerful tool for identifying the most common types of bonding in a material, whether they are covalent, ionic, metallic, or weakly bound.

A negative Cauchy pressure indicates a nonmetallic and brittle material, whereas a positive value denotes metallic and ductile properties. Positive Cauchy pressure of BeHfO<sub>3</sub> indicates its metallic characteristics and ductility. Brittleness is determined by whether the B/G is equal to or greater than 1.75. In contrast, ductile qualities are exhibited by a material with a B/G below 1.75. Using the PBE, RPBE, and PBE sol methods, the Pugh's ratio (B/G) in these calculations was found to be 0.69, 0.75, and 0.72, respectively. On the basis of these results, it appears that the substance is ductile. The fact that our present calculations are supported by the Cauchy pressure and Pugh's ratio indicates that they behave similarly. The ductile characteristics of BeHfO<sub>3</sub> perovskite, evidenced by its mechanical properties (such as positive Cauchy pressure, Pugh's ratio greater than 1.75), indicate its potential use in

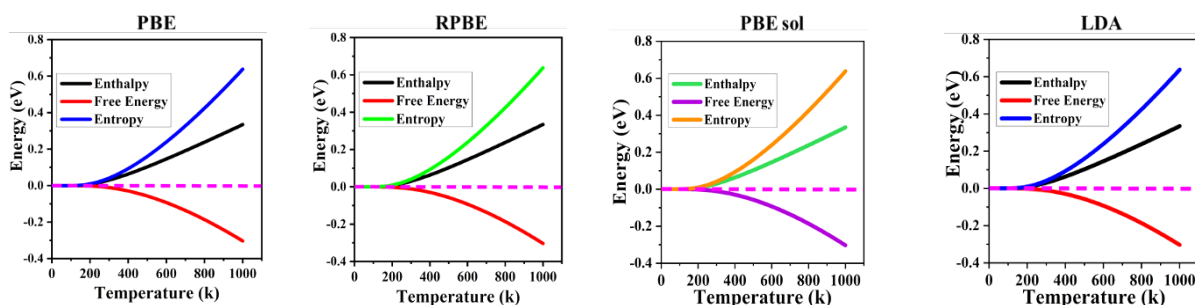
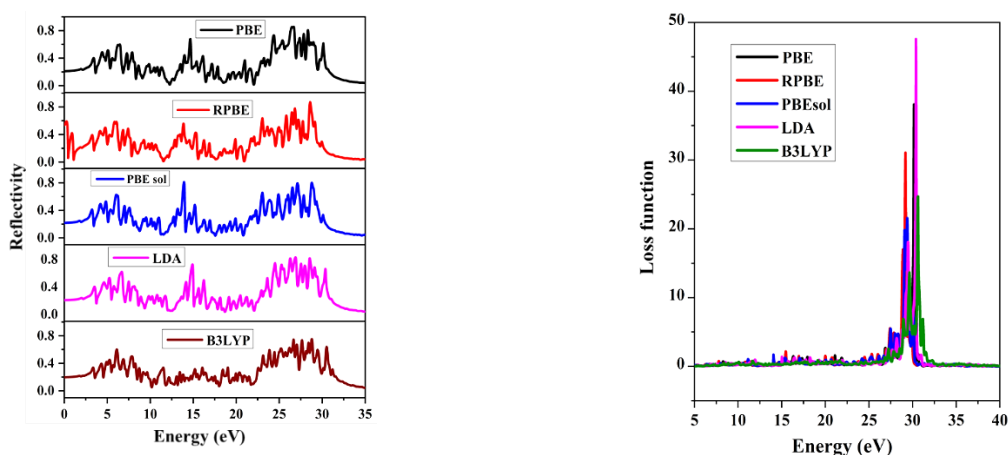
flexible electronic and mechanical domains. Ductility is an essential characteristic for materials designed for flexible or extensible devices, which allows them to withstand mechanical deformation without breaking. The mechanical flexibility of BeHfO<sub>3</sub>, together with its advantageous electrical and optical characteristics, positions it as a viable option for applications in next generation flexible optoelectronic and wearable devices.

The elevated bulk modulus of BeHfO<sub>3</sub> signifies increased elasticity, incompressibility, and rigidity compared to comparable materials. Its high shear modulus verifies the material's resistance to shear distortion and its robustness under shear stress [34]. Substances with Poisson's ratios approaching 0.5 demonstrate poor bonding, whereas lower values signify stiffer and more robust atomic connections. BeHfO<sub>3</sub> that exhibits Poisson ratios of 0.17, 0.19, and 0.21, indicates robust atomic bonding and elevated stiffness [35]. The universal anisotropy factor quantifies the changes in stiffness among crystallographic orientations. A number of 1 signifies isotropic elastic characteristics, but values less than 1 imply anisotropy.



**Table 5.** Elastic constants, Cauchy pressure, modulus of bulk, Young, Shear, (B/G), Poisson's ratio and anisotropy factor.

Method	C <sub>11</sub>	C <sub>12</sub>	C <sub>44</sub>	C <sub>12</sub> -C <sub>44</sub>	B	Y	G	B/G	$\nu$	A
PBE	12.86	77.44	58.12	19.32	34.01	282.11	48.93	0.69	0.17	0.30
RPBE	15.21	75.18	57.34	17.84	35.05	249.93	46.48	0.75	0.19	0.38
PPBESol	14.11	71.29	57.93	13.36	36.15	276.65	49.84	0.72	0.21	0.23

**Figure 5.** Enthalpy, entropy, free energy of BeHfO<sub>3</sub> in (a) PBE, (b) RPBE, (c) PBEsol and (d) LDA methods.**Figure 6.** (a) Optical reflectivity and (b) Loss function of the BeHfO<sub>3</sub> crystal.

The anisotropy index of BeHfO<sub>3</sub>, measuring 0.30, 0.38, and 0.23, indicates directional discrepancies in its elastic characteristics, encompassing stiffness [36]. External pressure or strain markedly affects the mechanical characteristics of perovskite materials, such as BeHfO<sub>3</sub>. Pressure or epitaxial strain can influence elastic constants, bulk modulus, and shear modulus, frequently increasing mechanical stability by diminishing structural distortions and increasing bond strength. In the case of BeHfO<sub>3</sub>, external modulation, such as compressive or tensile stress, can stabilize the perovskite phase by modifying the lengths and angles of the Hf-O and Be-O link, which influences the lattice dynamics and resistance to deformation. Consequently, strain engineering presents a feasible approach to enhance the structural integrity and mechanical efficacy of BeHfO<sub>3</sub>, possibly enhancing its use in functional devices.

### 3.4. Thermo-physical features

Entropy is a crucial and significant factor in the fields of physics, chemistry, and many other scientific disciplines that span different fields. Based on thermodynamic principles, a highly organized system will have a marginal entropy value [37]. The statistics illustrated in Figures 5a-d demonstrate that the entropy at 1000 K corresponds to a value of 0.5 eV. This suggests that BeHfO<sub>3</sub> may have a reduced level of instability or molecular disturbances. Excluding mechanical effort, the interplay of thermal energy and the environment, elucidated by enthalpy [38], ranging from 0.01 to 0.45 eV at temperatures

between 200 and 1000 K, is illustrated in Figures 5a-d. The variability in free energy determines the transformation pathway and the maximum effort achievable in thermal processes, such as chemical reactions [39]. Our empirical findings indicate that the free energy of the BeHfO<sub>3</sub> crystal starts at 0.02 eV at 190 K and increases steadily to 0.40 eV at 1000 K, as shown in Figures 5a-d. Heat capacity measures the amount of warmth required to change the temperature of a material, reflecting its ability to absorb or release energy. Figure S5a-d (ESI) demonstrates that BeHfO<sub>3</sub> attains its maximum heat capacity at 1000 K, showcasing varying energy levels evaluated using different methodologies.

### 3.5. Optical properties

A magnitude of 0.1 eV Gaussian smearing has been used across all computational approaches to explore the optical characteristics of the BeHfO<sub>3</sub> [40]. A material's reflectivity- its capacity to return energy or light to its source- is fundamental for comprehending its opacity, translucency, or transparency [41]. A notable increase in reflectance from 0.23 eV to 30 eV for BeHfO<sub>3</sub> is demonstrated by the results 0.85, 0.88, 0.82, 0.85, and 0.75 eV showed significant amounts of reflection in different methods shown in Figure 6a. An important optical feature, the energy loss function affects optoelectronic efficiency throughout both the low and high photon energy ranges [42]. According to Figure 6b, the LDA technique results in the largest energy loss for BeHfO<sub>3</sub>, whereas PBEsol yields the least. Choosing

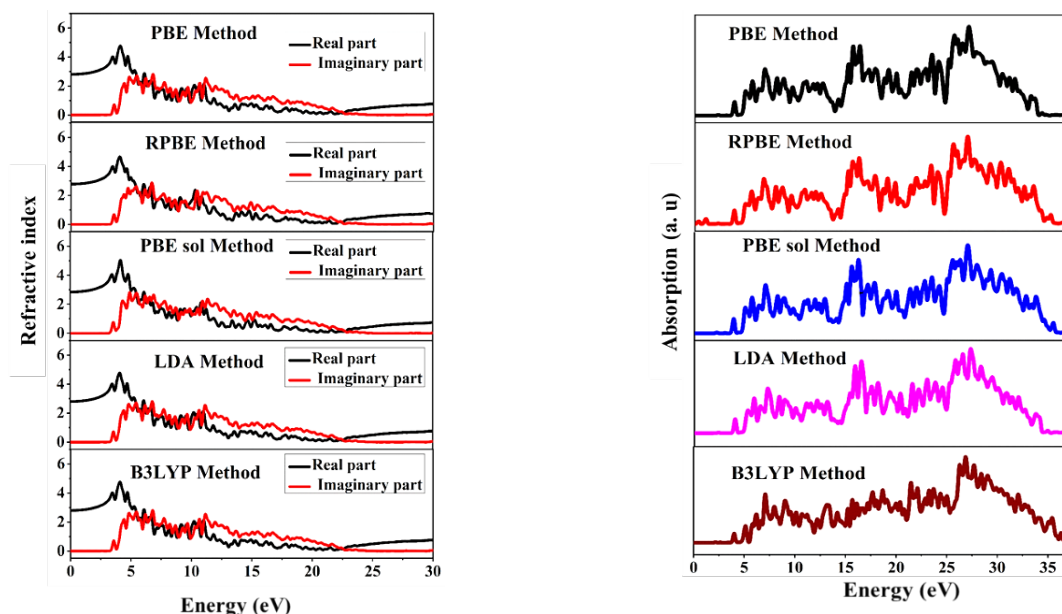


Figure 7. (a) Refraction index and (b) absorption curve of the BeHfO<sub>3</sub> crystal.

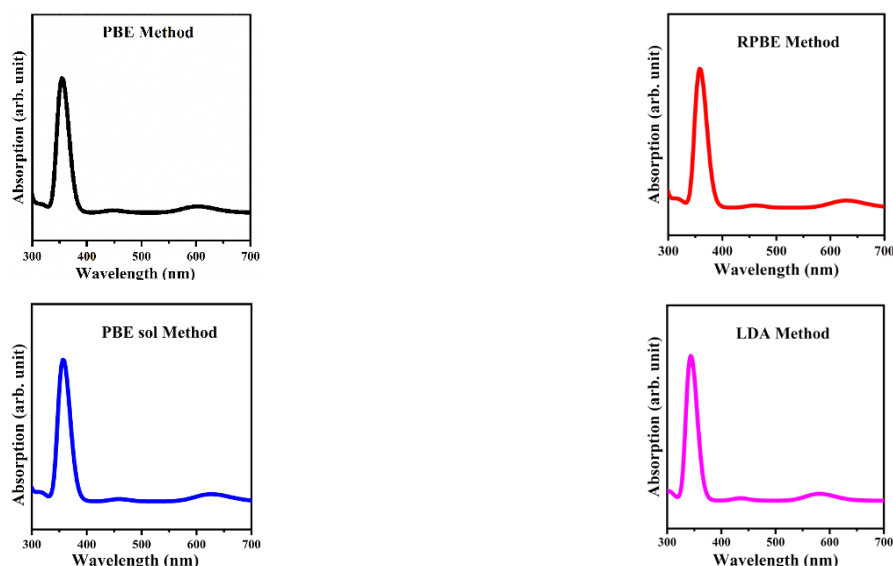


Figure 8. Wavelength-dependent absorption curve of BeHfO<sub>3</sub> crystal in (a) PBE, (b) RPBE, (c) PBEsol, and (d) LDA methods.

computational methods to reliably forecast the optical characteristics of BeHfO<sub>3</sub> requires this understanding.

The capacity of a substance to carry light is measured by its optical conductivity [43]. The actual component of BeHfO<sub>3</sub> is visible in Figure S6a (ESI) and is dominant up to 11.0 eV, after which it steadily drops by 30 eV. The energy absorption through electron-material contacts is shown by the fictitious part being greater than the real component after 11.0 eV.

An essential step in comprehending and creating optically customized materials is the estimation of electric dipoles, which are dielectric functions [44]. From 0 to 5.0 eV, the real component of BeHfO<sub>3</sub> is greater than the imaginary component, as shown in Figure S6b (ESI). However, as the energy approaches 30.0 eV, the real component diminishes. In the range of 5.0 to 30.0 eV, the imaginary part is larger than the actual part. The dielectric response of BeHfO<sub>3</sub> perovskite is comparatively elevated in relation to several established halide perovskites. An elevated dielectric constant is beneficial, since it improves charge carrier screening, diminishes exciton

binding energy, and promotes effective charge separation essential elements for enhancing the performance of optoelectronic devices, including solar cells, photodetectors, and light-emitting diodes. In contrast to some halide perovskites that exhibit environmental instability and lead toxicity, BeHfO<sub>3</sub> presents a potentially more stable and nontoxic alternative with an advantageous dielectric profile, rendering it a promising material for practical and enduring optoelectronic applications.

The refractive index plays a vital role in optics, indicating the interaction of light with various materials [45]. Figure 7a illustrates a negative correlation between the real and imaginary components in BeHfO<sub>3</sub>, while the real part was higher from 0.0 to 5.0 eV, followed by a decrease at 30 eV. The reliable characteristics of BeHfO<sub>3</sub> in terms of its absorption and refractive properties have significant implications for the advancement of new optical phenomena.

### 3.5.1. Optical absorption

Absorption features transpires when objects consume electromagnetic frequencies, delivering energetic to molecules or atoms, resulting in a boost of their power levels [46,47]. Figure 7b illustrates that BeHfO<sub>3</sub> displays a consistent absorption pattern across all methodologies, spanning range from 0 to 35 eV. The substance captures light within the visible spectrum (1.78 to 4.14 eV or 300 to 700 nm), exhibiting a maximum absorption of around 3.5 eV. Additionally, significant absorption spikes are seen in the ultraviolet (UV) range, with the most prominent rise at 24.5 eV, indicating BeHfO<sub>3</sub>'s ability to hold onto photons in both the visible and UV ranges.

Furthermore, Figures 8a-d illustrate the absorption coefficient curve of BeHfO<sub>3</sub> that varies with wavelength, employing the methodologies PBE, RPBE, PBEsol, LDA and B3LYP (Figure S8, ESI). The curves exhibit many different absorption maxima throughout the visible spectrum, covering wavelengths from 300 to 700 nm. The calculated maximum absorption wavelengths of BeHfO<sub>3</sub> are about 356, 360, 358, 344, and 309 nm for the corresponding techniques. These wavelengths correlate to the exact areas where BeHfO<sub>3</sub> exhibits its most significant light absorption.

The significant ultraviolet (UV) absorption of BeHfO<sub>3</sub> makes it a good option for UV detector use. Sensitive and selective UV detectors need materials that can easily catch and transform UV rays. The stability and electrical qualities of BeHfO<sub>3</sub> also make it a good candidate for UV photodetectors, which means it might be used in future optoelectronic devices that work in the UV region. The existence of these peaks signifies that BeHfO<sub>3</sub> has certain absorption properties at these exact wavelengths. Furthermore, the material has considerable sensitivity to visible light, as indicated by its pronounced absorption peaks, establishing BeHfO<sub>3</sub> as a very attractive option for optoelectronic and photocatalytic applications, where effective manipulation and detection of visible light are essential [48-50].

## 4. Conclusions

This investigation employs various computational techniques, such as PBE, RPBE, PBEsol, LDA, HSE06 and B3LYP, to evaluate the bandgap energy, uncovering an indirect bandgap feature with computed values of 0.873, 0.887, 0.780, 0.890, 1.71 and 2.295 eV, accordingly. To gain deeper insight into the electronic structure, a comprehensive and partial density of states (DOS) analysis was performed to elucidate the contributions of atomic orbitals to the electronic properties of the compound. Furthermore, bonding characteristics were analyzed through Mulliken population charge estimations, providing a detailed understanding of the charge distribution and interactions within the crystal lattice. The crystalline structure of BeHfO<sub>3</sub> demonstrates remarkable mechanical robustness, which is characterized by its ductility, elastic anisotropy, and significant mechanical and thermal stability. These properties indicate a high degree of structural resistance under various conditions. Additionally, the optical properties of BeHfO<sub>3</sub> underscore its promise for photocatalytic applications, owing to its chop bandgap and remarkable absorption aptitude throughout the visible and ultraviolet exposure range. It additionally highlights BeHfO<sub>3</sub> as a notable contender in the realm of semiconducting photocatalysts, suggesting its potential utility in sophisticated optoelectronic systems. An in-depth look offers a basic understanding of versatile characteristics, enabling its incorporation into various technological fields.

## Acknowledgements

The authors thank the Department of Physics and ICT, European University of Bangladesh, Dhaka-1216, for providing facilities and support to carry out this research.

## Supporting information

Electronic supplementary information (ESI) available: Figure S1. Band structure of BeHfO<sub>3</sub> using the B3LYP method. Figure S2. Band structure of BeHfO<sub>3</sub> using the HSE06 method. Figure S3. DOS and PDOS of BeHfO<sub>3</sub> using the B3LYP method. Figure S4. Different partial states of BeHfO<sub>3</sub> using the B3LYP method. Figure S5. Heat capacity of BeHfO<sub>3</sub> in (a) PBE, (b) RPBE (c) PBE sol and (d) LDA methods. Figure S6. (a) Optical conductivity and (b) Dielectric function of BeHfO<sub>3</sub> in GGA using the PBE, RPBE, PBE sol, LDA and B3LYP methods. Figure S7. Optical absorption of BeHfO<sub>3</sub> using B3LYP method.

## Disclosure statement

Conflict of interests: The authors declare that they have no conflict of interest. Ethical approval: All ethical guidelines have been adhered. Sample availability: Samples of the compounds are available from the author.

## CRediT authorship contribution statement

Conceptualization: Md. Al Masud, Md. Rajib Munshi; Methodology: Md. Al Masud, Md. Rajib Munshi; Software: Md. Rajib Munshi; Validation: Md. Al Masud, Md. Rajib Munshi; Formal Analysis: Md. Al Masud, Md. Rajib Munshi, Tanvir Chowdhury, Mita Chakraborty, Rakibul Islam; Investigation: Md. Al Masud, Md. Rajib Munshi, Tanvir Chowdhury, Mita Chakraborty, Rakibul Islam; Resources: Md. Rajib Munshi; Data Curation: Md. Rajib Munshi; Writing - Original Draft: Md. Al Masud, Md. Rajib Munshi, Tanvir Chowdhury, Mita Chakraborty, Rakibul Islam; Writing - Review and Editing: Md. Al Masud, Md. Rajib Munshi, Tanvir Chowdhury, Mita Chakraborty, Rakibul Islam; Visualization: Md. Rajib Munshi; Funding acquisition: Md. Rajib Munshi; Supervision: Md. Rajib Munshi; Project Administration: Md. Rajib Munshi.

## ORCID and Email

Md Al Masud

 [almasud2509@gmail.com](mailto:almasud2509@gmail.com)

 <https://orcid.org/0009-0006-2109-6947>

Md. Rajib Munshi

 [razibmunshi@eub.edu.bd](mailto:razibmunshi@eub.edu.bd)

 <https://orcid.org/0000-0002-5594-1014>

Tanvir Chowdhury

 [tanvirchowdhury2@gmail.com](mailto:tanvirchowdhury2@gmail.com)

 <https://orcid.org/0009-0002-9434-2433>

Mita Chakraborty

 [mita76h@gmail.com](mailto:mita76h@gmail.com)

 <https://orcid.org/0009-0009-9038-7301>

Rakibul Islam

 [rakib133@gmail.com](mailto:rakib133@gmail.com)

 <https://orcid.org/0009-0005-4294-7280>

## References

- [1]. Deng, M.; Shen, S.; Wang, X.; Zhang, Y.; Xu, H.; Zhang, T.; Wang, Q. Controlled synthesis of AgInS<sub>2</sub> nanocrystals and their application in organic-inorganic hybrid photodetectors. *CrystEngComm*. **2013**, *15* (33), 6443.
- [2]. Holladay, J.; Hu, J.; King, D.; Wang, Y. An overview of hydrogen production technologies. *Catalysis Today* **2009**, *139* (4), 244-260.
- [3]. Sen, S. K.; Munshi, M. R.; Kumar, A.; Mortuza, A. A.; Manir, M. S.; Islam, M. A.; Hossain, M. N.; Hossain, M. K. Structural, optical, magnetic, and enhanced antibacterial properties of hydrothermally synthesized Sm-incorporating  $\alpha$ -MoO<sub>3</sub>2D-layered nanoplates. *RSC Adv*. **2022**, *12* (53), 34584-34600.
- [4]. Liu, Y.; Zhang, W.; Wang, B.; Sun, L.; Li, F.; Xue, Z.; Zhou, G.; Liu, B.; Nian, H. Theoretical and Experimental Investigations on High Temperature Mechanical and Thermal Properties of BaZrO<sub>3</sub>. *Ceram. Int*. **2018**, *44* (14), 16475-16482.
- [5]. Feng, Z.; Hu, H.; Cui, S.; Bai, C. First-principles study of optical properties of SrZrO<sub>3</sub> in cubic phase. *Solid State Communications* **2008**, *148* (9-10), 472-475.



- [6]. Islam, M. T.; Kumer, A.; Chakma, U.; Howlader, D. A Computational Investigation of Electronic Structure and Optical Properties of AlCuO<sub>2</sub> and AlCu<sub>0.96</sub>Fe<sub>0.04</sub>O<sub>2</sub>: A First Principle Approach. *Orbital: Electron J. Chem.* **2021**, *13* (1).
- [7]. Amisi, S.; Bousquet, E.; Katcho, K.; Ghosez, P. First-principles study of structural and vibrational properties of SrZrO<sub>3</sub>. *Phys. Rev. B* **2012**, *85* (6), 064112.
- [8]. Amisi, S. First-principles study of structural and vibrational properties of SrHfO<sub>3</sub> compared to SrZrO<sub>3</sub>. *Computational Condensed Matter.* **2019**, *20*, e00383.
- [9]. Kang, S. G.; Sholl, D. S. First-principles investigation of chemical stability and proton conductivity of M-doped BaZrO<sub>3</sub> (M=K, Rb, and Cs). *J. Am. Ceram. Soc.* **2017**, *100* (7), 2997–3003.
- [10]. Liu, Q.; Liu, Z.; Feng, L.; Tian, H. Mechanical, electronic, chemical bonding and optical properties of cubic BaHfO<sub>3</sub>: First-principles calculations. *Physica. B: Condensed Matter.* **2010**, *405* (18), 4032–4039.
- [11]. Husain, M.; Albalawi, H.; Huwayz, M. A.; Al Saqri, N. a.; Khan, R.; Rahman, N. Computational insight into the fundamental physical properties of ternary ABX<sub>3</sub> chloroperovskites compounds using the DFT approach. *Phys. Scr.* **2023**, *98* (10), 105935.
- [12]. Rahman, N.; Husain, M.; Tirth, V.; Algahtani, A.; Algahtani, H.; Al-Mughanam, T.; Alghtani, A. H.; Khan, R.; Sohail, M.; Khan, A. A.; Azzouz-Rached, A.; Khan, A. Appealing perspectives of the structural, electronic, elastic and optical properties of LiRCl<sub>3</sub> (R = Be and Mg) halide perovskites: a DFT study. *RSC. Adv.* **2023**, *13* (27), 18934–18945.
- [13]. Pasha, A. A.; Khan, H.; Sohail, M.; Rahman, N.; Khan, R.; Alsalmi, O. H.; Abduvalieva, D.; Abualnaja, K. M.; El Jery, A.; Addrery, M. Computational study of the physical characteristics of Si-based oxide perovskites for energy generation using DFT. *Mater. Adv.* **2023**, *4* (24), 6645–6654.
- [14]. Haoui, A.; Elchikh, M.; Hiads, S. Mechanical, optoelectronic and thermoelectric properties of the transition metal oxide perovskites YScO<sub>3</sub> and LaScO<sub>3</sub>: First principle calculation. *Physica. B: Condensed Matter.* **2023**, *654*, 414732.
- [15]. Shah, S. A.; Husain, M.; Rahman, N.; Sohail, M.; Khan, R.; Khan, A. A.; Ullah, A.; Abdelmohsen, S. A.; Abdelbacki, A. M.; El-Sabrou, A. M.; Elansary, H. O.; Khan, A. Insight into the exemplary structural, elastic, electronic and optical nature of GaBeCl<sub>3</sub> and InBeCl<sub>3</sub>: a DFT study. *RSC. Adv.* **2022**, *12* (13), 8172–8177.
- [16]. Ullah, W.; Husain, M.; Rahman, N.; Sfina, N.; Elhadi, M.; Khan, R.; Sohail, M.; Azzouz-Rached, A.; Uzair, M.; Khan, A. A.; Khan, A. Computational Analysis of Structural, Elastic, and Optoelectronic Properties of Silicon-Based XSiO<sub>3</sub> (X = Sc and Y) Oxide Perovskite Compounds Employing the Density Functional Theory Approach. *Silicon* **2024**, *16* (7), 3021–3032.
- [17]. Husain, M.; Rahman, N.; Albalawi, H.; Ezzine, S.; Amami, M.; Zaman, T.; Rehman, A. U.; Sohail, M.; Khan, R.; Khan, A. A.; Tahir, Khan, A. Examining computationally the structural, elastic, optical, and electronic properties of CaQCl<sub>3</sub> (Q = Li and K) chloroperovskites using DFT framework. *RSC. Adv.* **2022**, *12* (50), 32338–32349.
- [18]. Shah, S. A.; Husain, M.; Rahman, N.; Sohail, M.; Khan, R.; Alataway, A.; Dewidar, A. Z.; Elansary, H. O.; Abu El Maati, L.; Yessoufou, K.; Ullah, A.; Khan, A. Insight into the Structural, Electronic, Elastic, Optical, and Magnetic Properties of Cubic Fluoroperovskites ABF<sub>3</sub> (A = Ti, B = Nb, V) Compounds: Probed by DFT. *Materials* **2022**, *15* (16), 5684.
- [19]. Khan, M. S.; Sohail, M.; Rahman, N.; Khan, R.; Ali, H. E.; Jamil, J.; Abdullaeva, B. S.; Abualnaja, K. M.; Alosaimi, G.; Khairy, Y.; Algarni, H. Investigation of the structural, electronic, magnetic, mechanical, and optical properties of calcium-based CaJO<sub>3</sub> (J = Mn, Ru) perovskites: A first-principle computations. *Chem. Pap.* **2024**, *79* (1), 95–105.
- [20]. Alrashidi, K. A.; Dixit, A.; Nazir, K.; Khara, E. A.; Mohammad, S.; Manzoor, M.; Khan, R.; Sharma, R. A DFT Approach to Insight on the Structural, Optoelectronic and Thermoelectric Properties of Cubic Perovskites YXO<sub>3</sub> (X = Ga, In) for Renewable Energy Applications. *J. Inorg. Organomet. Polym.* **2024**, *35* (3), 1764–1778.
- [21]. Akhtar, S.; Alay-e-Abbas, S. M.; Abbas, S. M.; Arshad, M. I.; Batool, J.; Amin, N. First-principles evaluation of electronic and optical properties of (Mo, C) codoped BaHfO<sub>3</sub> for applications in photocatalysis. *Journal of Applied Physics* **2018**, *123* (16).
- [22]. Bouhemadou, A.; Djabi, F.; Khenata, R. First Principles Study of Structural, Elastic, Electronic and Optical Properties of the Cubic Perovskite BaHfO<sub>3</sub>. *Phys. Lett. A* **2008**, *372* (24), 4527–4531.
- [23]. Ahmed, S.; Zulfiqar, W.; Javed, F.; Arshad, H.; Abbas, G.; Laref, A.; Alay-e-Abbas, S. M. Accurate first-principles evaluation of structural, electronic, optical and photocatalytic properties of BaHfO<sub>3</sub> and SrHfO<sub>3</sub> perovskites. *Journal of Alloys and Compounds* **2022**, *892*, 162071.
- [24]. Feng, L.; Liu, Z.; Liu, Q.; Tian, H. First-principles study of electronic and optical properties of Pbnm orthorhombic SrHfO<sub>3</sub>. *Computational Materials Science* **2010**, *50* (2), 454–458.
- [25]. Muscat, J.; Wander, A.; Harrison, N. M. On the prediction of band gaps from hybrid functional theory. *Chem. Phys. Lett.* **2001**, *342*, 397–401.
- [26]. Islam, J.; Hossain, A. K. Narrowing band gap and enhanced visible-light absorption of metal-doped non-toxic CsSnCl<sub>3</sub> metal halides for potential optoelectronic applications. *RSC. Adv.* **2020**, *10* (13), 7817–7827.
- [27]. Munshi, M. R.; Masud, M. A.; Khatun, A. Structural, electronic, mechanical, thermodynamic and optical properties of oxide perovskite BeZrO<sub>3</sub>: a DFT study. *Phys. Scr.* **2024**, *99* (8), 085904.
- [28]. Zahan, M. S.; Munshi, M. R.; Rana, M. Z.; Al Masud, M. Theoretical insights on geometrical, mechanical, electronic, thermodynamic and photocatalytic characteristics of RaTiO<sub>3</sub> compound: A DFT investigation. *Computational Condensed Matter.* **2023**, *36*, e00832.
- [29]. Md. Rajib Munshi; Md. Zuel Rana; Sapan Kumar Sen; Md. Ruhul Amin Foisal; Md. Hazrat Ali, Theoretical investigation of structural, electronic, optical and thermoelectric properties of GaAgO<sub>2</sub> based on Density Functional Theory (DFT): Two approach. *World. J. Adv. Res. Rev.* **2022**, *13* (2), 279–291.
- [30]. Sohail, M.; Husain, M.; Rahman, N.; Althubeiti, K.; Algethami, M.; Khan, A. A.; Iqbal, A.; Ullah, A.; Khan, A.; Khan, R. First-principal investigations of electronic, structural, elastic and optical properties of the fluoroperovskite TlLF<sub>3</sub> (L = Ca, Cd) compounds for optoelectronic applications. *RSC. Adv.* **2022**, *12*, 7002–7008.
- [31]. Munshi, M. R.; Sen, S. K.; Rana, M. Z. Electronic, thermodynamic, optical and photocatalytic properties of GaAgO<sub>2</sub> and AlAgO<sub>2</sub> compounds scrutinized via a systemic hybrid DFT. *Computational Condensed Matter.* **2023**, *34*, e00778.
- [32]. Rana, M. Z.; Munshi, M. R.; Al Masud, M.; Zahan, M. S. Structural, electronic, optical and thermodynamic properties of AlAuO<sub>2</sub> and AlAu<sub>0.94</sub>Fe<sub>0.06</sub>O<sub>2</sub> compounds scrutinized by density functional theory (DFT). *Heliyon* **2023**, *9* (11), e21405.
- [33]. Chen, X.; Zeng, M.; Wang, R.; Mo, Z.; Tang, B.; Peng, L.; Ding, W. First-principles study of (Ti<sub>1-x</sub>Gx)Si<sub>3</sub> phases with the hexagonal D88 structure: Elastic properties and electronic structure. *Computational Materials Science* **2012**, *54*, 287–292.
- [34]. Rahman, N.; Husain, M.; Yang, J.; Sajjad, M.; Murtaza, G.; Ul Haq, M.; Habib, A.; Zulfiqar, Rauf, A.; Karim, A.; Nisar, M.; Yaqoob, M.; Khan, A. First principle study of structural, electronic, optical and mechanical properties of cubic fluoro-perovskites: (CdXF<sub>3</sub>, X = Y, Bi). *Eur. Phys. J. Plus.* **2021**, *136* (3).
- [35]. Sohail, M.; Husain, M.; Rahman, N.; Althubeiti, K.; Algethami, M.; Khan, A. A.; Iqbal, A.; Ullah, A.; Khan, A.; Khan, R. First-principal investigations of electronic, structural, elastic and optical properties of the fluoroperovskite TlLF<sub>3</sub> (L = Ca, Cd) compounds for optoelectronic applications. *RSC. Adv.* **2022**, *12* (12), 7002–7008.
- [36]. Al-Qaisi, S.; Mebed, A. M.; Mushtaq, M.; Rai, D. P.; Alrebbi, T. A.; Sheikh, R. A.; Rached, H.; Ahmed, R.; Faizan, M.; Bouzgarrou, S.; Javed, M. A. A theoretical investigation of the lead-free double perovskites halides Rb<sub>2</sub>XCl<sub>6</sub> (X = Se, Ti) for optoelectronic and thermoelectric applications. *J. Comput. Chem.* **2023**, *44* (19), 1690–1703.
- [37]. Rahman, S.; Hussain, A.; Noreen, S.; Bibi, N.; Arshad, S.; Rehman, J. U.; Tahir, M. B. Structural, electronic, optical and mechanical properties of oxide-based perovskite AB<sub>3</sub>O<sub>3</sub> (A = Cu, Nd and B = Sn, Sc): A DFT study. *J. Solid State Chem.* **2023**, *317*, 123650.
- [38]. Salma, M.; Atikur Rahman, M. Study of structural, elastic, electronic, mechanical, optical and thermodynamic properties of NdPb<sub>3</sub> intermetallic compound: DFT based calculations. *Computational Condensed Matter.* **2018**, *15*, 42–47.
- [39]. Rehman, J. U.; Usman, M.; Tahir, M. B.; Hussain, A.; Rashid, M. Investigation of Structural, Electronics, Optical, Mechanical and Thermodynamic Properties of YRu<sub>2</sub>P<sub>2</sub> Compound for Superconducting Application. *J. Supercond. Nov. Magn.* **2021**, *34* (12), 3089–3097.
- [40]. Colmenero, F.; Timón, V. Study of the structural, vibrational and thermodynamic properties of natroxalate mineral using density functional theory. *Journal of Solid State Chemistry* **2018**, *263*, 131–140.
- [41]. Ferrari, A. M.; Orlando, R.; Rérat, M. *Ab Initio* Calculation of the Ultraviolet-Visible (UV-vis) Absorption Spectrum, Electron-Loss Function, and Reflectivity of Solids. *J. Chem. Theory. Comput.* **2015**, *11* (7), 3245–3258.
- [42]. Islam, M. A.; Islam, J.; Islam, M. N.; Sen, S. K.; Hossain, A. K. Enhanced ductility and optoelectronic properties of environment-friendly CsGeCl<sub>3</sub> under pressure. *AIP. Advances* **2021**, *11* (4), 045014.
- [43]. Kora, H. H.; Taha, M.; Abdelwahab, A.; Farghali, A. A.; El-dek, S. I. Effect of pressure on the geometric, electronic structure, elastic, and optical properties of the normal spinel MgFe<sub>2</sub>O<sub>4</sub>: a first-principles study. *Mater. Res. Express.* **2020**, *7* (10), 106101.
- [44]. Al-Qaisi, S.; Mushtaq, M.; Alzahrani, J. S.; Alkhalidi, H.; Alrowaili, Z.; Rached, H.; Haq, B. U.; Mahmood, Q.; Al-Buriah, M.; Morsi, M. First-principles calculations to investigate electronic, structural, optical, and thermoelectric properties of semiconducting double perovskite Ba<sub>2</sub>YBiO<sub>6</sub>. *Micro. Nanostructures* **2022**, *170*, 207397.
- [45]. Dey, A.; Sharma, R.; Dar, S. A.; Wani, I. H. Cubic PbGeO<sub>3</sub> perovskite oxide: A compound with striking electronic, thermoelectric and optical properties, explored using DFT studies. *Computational Condensed Matter.* **2021**, *26*, e00532.

- [46]. Munshi, M. R.; Zahan, M. S.; Rana, M. Z.; Masud, M. A.; Rashid, R.; Azad, M. A. First principles prediction of structural, electronic, mechanical, thermodynamic, optical and photocatalytic properties of  $\text{In(X)O}_2$ , where X= Cu, Ag crystal scrutinized by hybrid DFT. *Computational Condensed Matter*. **2024**, *38*, e00884.
- [47]. Wesch, W.; Rensberg, J.; Schmidt, M.; Wendler, E. Damage evolution in  $\text{LiNbO}_3$  due to electronic energy deposition below the threshold for direct amorphous track formation. *J. Appl. Phys.* **2019**, *126*, 125105.
- [48]. Munshi, M. R.; Masud, M. A.; Rahman, M.; Khatun, M. R.; Mian, M. F. First principles prediction of geometrical, electronic, mechanical, thermodynamic, optical and photocatalytic properties of  $\text{RaZrO}_3$  scrutinized by DFT investigation. *Computational Condensed Matter*. **2024**, *38*, e00865.
- [49]. Halim, S. A. TD-DFT calculations, electronic structure, natural bond orbital analysis, nonlinear optical properties electronic absorption spectra and antimicrobial activity application of new bis-spiropipridinon/pyrazole derivatives. *Eur. J. Chem.* **2018**, *9* (4), 287–302.
- [50]. Ephraim Babu, K.; Veeraiah, A.; Tirupathi Swamy, D.; Veeraiah, V. First-principles study of electronic and optical properties of cubic perovskite  $\text{CsSrF}_3$ . *Mater. Sci-Pol.* **2012**, *30* (4), 359–367.



Copyright © 2025 by Authors. This work is published and licensed by Atlanta Publishing House LLC, Atlanta, GA, USA. The full terms of this license are available at <https://www.eurjchem.com/index.php/eurjchem/terms> and incorporate the Creative Commons Attribution-Non Commercial (CC BY NC) (International, v4.0) License (<http://creativecommons.org/licenses/by-nc/4.0>). By accessing the work, you hereby accept the Terms. This is an open access article distributed under the terms and conditions of the CC BY NC License, which permits unrestricted non-commercial use, distribution, and reproduction in any medium, provided the original work is properly cited without any further permission from Atlanta Publishing House LLC (European Journal of Chemistry). No use, distribution, or reproduction is permitted which does not comply with these terms. Permissions for commercial use of this work beyond the scope of the License (<https://www.eurjchem.com/index.php/eurjchem/terms>) are administered by Atlanta Publishing House LLC (European Journal of Chemistry).